Magnon spectrum of transition-metal oxides: Calculations including long-range magnetic interactions using the LSDA + U method

F. Essenberger,[1] S. Sharma,[1] J. K. Dewhurst,[1] C. Bersier,[1] F. Cricchio,[2] L. Nordström,[2] and E. K. U. Gross[1]

[1]*Max-Planck-Institut für Mikrostrukturphysik, Weinberg 2, DE-06120 Halle, Germany*

[2]*Department of Physics, Uppsala University, P.O.Box 530, SE-75121 Uppsala, Sweden*

(Received 9 August 2011; published 18 November 2011)

We present LSDA + U calculations of the magnon frequencies of transition-metal monoxides (TMOs) using the frozen magnon approach. We systematically vary U to investigate the effect of the on-site Coulomb repulsion on various properties such as the gap, the magnetic moment, and the magnon energies. For all TMOs, a similar behavior of the gap and moment with respect to U is found: the gaps start to increase linear and saturate for large U. The moment is enhanced by $\approx 0.4\ \mu_B$ towards the pure spin limit. Magnon energies are strongly suppressed on increasing the on-site Coulomb repulsion. The reason for this behavior is related to charge localization.

DOI: 10.1103/PhysRevB.84.174425 PACS number(s): 75.30.−m, 71.10.−w, 72.80.Ga

I. INTRODUCTION

Among the strongly correlated materials, TMOs are particularly interesting as these materials are prototypical Mott insulators (with strongly localized d electrons). Experimentally, TMOs are known to be antiferromagnetic (AFM) insulators with a gap ranging from 2.6 (FeO) to 4.3 eV (NiO). On going above the Néel temperature, the long-range AFM order is lost but the TMOs still remain insulating in nature with very little change in the value of the gap. This indicates that the occurrence of the gap in TMOs is independent of the long-range spin order. The explanation why TMOs are insulating was formulated by Mott.[1] He showed that the electron hopping can be entirely dominated by a large on-site repulsion U, which gives rise to lower and upper Hubbard bands separated by a gap (of the order of U). Conventional density functional theory (DFT) calculations, using local/semilocal exchange-correlation functionals, cannot capture such strong Mott correlations;[2] Mott insulators when treated with these types of exchange-correlation functionals and without any long-range magnetic order, show a metallic ground state. On explicit incorporation of AFM order, a small Slater-like gap (up to 90% smaller than experiments) opens in some of the TMOs (NiO and FeO) while others remain metallic.[3]

Over the years, many ideas were developed to treat these strongly correlated systems. Among them, most prominent within the frame work of DFT are self-interaction corrected local spin density approximation (LSDA),[4,5] hybrid functionals,[6–8] and LSDA + U. Out of these methods, LSDA + U is particularly useful as it is computationally less demanding and hence can easily be used for larger systems of modern-day interest. Furthermore, with LSDA + U it is possible to systematically increase the strength of the on-site repulsion in order to gain insight into the effect of Coulomb correlations. The first very simple version of LSDA + U was not rotationally invariant[9] and when applied to the TMOs, was able to solve the gap problem of pure LSDA. As a consequence LSDA + U became the method of choice for treating correlated materials.[10–12] The most general method containing two parameters (U the averaged screened Coulomb interaction and J the exchange interaction) was presented by Lichtenstein *et al.*,[13] rotationally averaged approaches[14–16] with only one parameter are also widely used. However, for small energy differences (μeV), the second parameter, J, may become important.[17]

Magnons are quantized, low-energy collective magnetic excitations and play an important role in the phase-diagram of high-T_c superconductors.[18,19] In fact, in the case of the cuprates, a simple empirical relation between the magnetic coupling constant and the critical temperature is found.[20–22] The Mott physics in these cuprates is similar to that in the TMOs,[9,23] but the chemical unit cells are much smaller for the latter. Hence, the TMOs can act as benchmark systems for undoped cuprates. With this in mind, we combine, in the present work, the LSDA + U method with the frozen magnon formalism to calculate the magnon spectrum of TMOs.

Many results have been published, studying the TMOs (especially NiO), with the LSDA + U method.[9,12,14,15,24–27] These works mainly revolve around the calculation of ground-state properties like gaps, moments, and density of states (DOS). Magnon spectra of various TMOs have also been calculated.[5,28–30] However, all these calculations have been performed using the so-called $J_1 J_2$ model in real space and as a result only the nearest- and next-nearest-neighbor magnetic interactions are taken into account. In this work, we systematically study the magnon spectra for the TMOs. With calculations performed using the Fourier transformed magnetic interactions; the upshot of which is that magnetic interactions with an infinite number of neighbors are accounted for. As in previous magnon calculations,[5,28,29] the present work also uses a frozen magnon approach, but at each point in the Brillouin zone (BZ), a fully self-consistent calculation is performed to accurately determine the total energies. Furthermore, a detailed investigation of the effect of Coulomb correlations on magnon energies as well as ground-state properties, like gaps and moments, is performed by systematically changing the value of U.

The paper is organized as follows: Sec. II contains the theoretical background for magnon calculations, a brief introduction to LSDA + U method is given and the general equation for the magnon energies (for any FM or AFM ground state) is derived. In Sec. III, the computational details are presented, followed by the results in Sec. IV.

II. THEORETICAL BACKGROUND

A. Formalism for magnons

1. Real-space formalism

There are two main ways of calculating magnons within the framework of DFT. The first one is the dynamical susceptibility method in which a spiral external field is applied to the system and the induced magnetic moment is calculated using linear response theory.[30–32] The second is based on the frozen magnon method;[33] in this approach, the magnetic interactions are mapped to a Heisenberg Hamiltonian of the form (atomic units are used throughout)

$$\hat{H}(t) = -\frac{1}{2}\sum_{i\neq j} J_{ij}\hat{\mathbf{M}}_i(t)\cdot\hat{\mathbf{M}}_j(t), \tag{1}$$

where the sum runs over all atoms, i, with on-site moment $\hat{\mathbf{M}}_i(t)$, defined as

$$\hat{\mathbf{M}}_i(t) = -\sum_{\alpha,\beta=1}^{2}\int_{V_i} d^3r\ \hat{\Psi}^{\dagger}_{\alpha}(\mathbf{r},t)\,\vec{\sigma}_{\alpha\beta}\hat{\Psi}_{\beta}(\mathbf{r},t), \tag{2}$$

where V_i is a volume enclosing the atom i, $\vec{\sigma}$ are the Pauli matrices and $\hat{\Psi}^{\dagger}_{\alpha}(\mathbf{r},t)$ are the the spinor-field operators in the Heisenberg picture. J_{ij} in Eq. (1) are the coupling constants[34] between two magnetic atoms located at $\mathbf{R}_i$ and $\mathbf{R}_j$. These coupling constants are real and symmetric ($J_{ij} = J_{ji}$). Since we are dealing with periodic systems, the J_{ij} are also invariant with respect to lattice-vector translations.

To study the magnetic modes of a system, the following equation of motion needs to be solved:

$$\left\langle\frac{d\hat{\mathbf{M}}_j(t)}{dt}\right\rangle = \sum_{i(\neq j)} J_{ij}\langle\hat{\mathbf{M}}_j(t)\times\hat{\mathbf{M}}_i(t)\rangle. \tag{3}$$

To solve this equation, certain approximations are made. The first is a type of mean-field approximation:

$$\begin{aligned}\langle\hat{\mathbf{M}}_j(t)\times\hat{\mathbf{M}}_i(t)\rangle &\approx \langle\hat{\mathbf{M}}_j(t)\rangle\times\langle\hat{\mathbf{M}}_i(t)\rangle \\ &= \mathbf{M}_i(t)\times\mathbf{M}_j(t).\end{aligned} \tag{4}$$

The approximation is valid for systems where the correlation hole of electrons on different lattice sites is small.[33] The second approximation is a restriction on the type of spin waves considered: (1) the angle θ_j that the on-site moment makes with the z axis is very small and time independent [$\theta_j(t) = \theta_j^0$ or $\theta_j(t) = \theta_j^0 + \pi$ and $\theta_j^0 \to 0$], (2) the magnitude M_i of the on-site magnetic moment is similarly assumed to be time independent, and (3) the azimuthal angle has the form

$$\phi_i^{\mathbf{q}}(t) = \mathbf{q}\cdot\mathbf{R}_i + \omega_{\mathbf{q}}t, \tag{5}$$

with $\mathbf{q}$ being the wavelength and $\omega_{\mathbf{q}}$ the frequency of the spin wave. With these assumptions the moment becomes

$$\mathbf{M}_i^{\mathbf{q}}(t) = M_i\begin{pmatrix}\cos\phi_i^{\mathbf{q}}(t)\sin\theta_i\\ \sin\phi_i^{\mathbf{q}}(t)\sin\theta_i\\ \cos\theta_i\end{pmatrix}, \tag{6}$$

as schematically illustrated in Fig. 1. The considered type of spin wave represents low-lying (small θ), collective (extended over the whole crystal) excitations of the ordered magnetic ground state, and the magnons are defined as the quantized modes of these excitations.

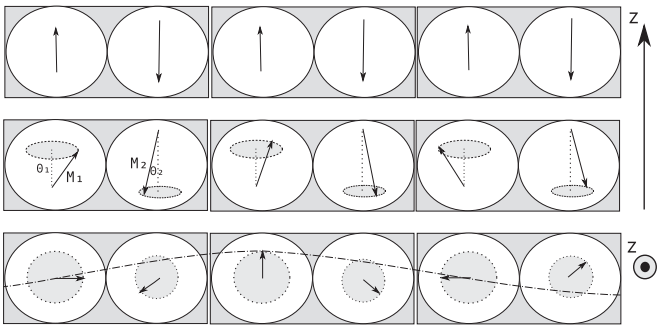

FIG. 1. AFM ground state (top row) and symmetry of the spin excitation (2nd and 3rd rows). The volume V_i in Eq. (2) for which the on-site moment is calculated is indicated by the white sphere.

Eqs. (4) and (6) together lead to the equations of motion for $\phi_i^{\mathbf{q}}(t)$ and θ_i:

$$\begin{aligned}\omega_{\mathbf{q}}\sin\theta_j = &\sum_{i(\neq j),} J_{ij}M_i[(\sin\theta_j\cos\theta_i)\\ &-\cos\theta_j\sin\theta_i\cos(\mathbf{q}\cdot\mathbf{R}_j - \mathbf{q}\cdot\mathbf{R}_i)]\end{aligned} \tag{7}$$

$$\sum_{i(\neq j),} J_{ij}M_i\sin\theta_i\sin(\mathbf{q}\cdot\mathbf{R}_j - \mathbf{q}\cdot\mathbf{R}_i) = 0. \tag{8}$$

Expanding Eq. (7) up to first order in θ_j^0 leads to

$$\theta_j^0\omega_{\mathbf{q}} = \sum_{i(\neq j),} J_{ij}M_i\left\{\theta_j^0 - \theta_i^0 A_j A_i \mathrm{Re}[e^{i\mathbf{q}\cdot(\mathbf{R}_j-\mathbf{R}_i)}]\right\}, \tag{9}$$

where the prefactor A_i is defined as

$$A_i := \begin{cases}1 & \text{if} \quad \theta_i \approx 0,\\ -1 & \text{if} \quad \theta_i \approx \pi.\end{cases} \tag{10}$$

For a FM, the prefactor is always $+1$ and for an AFM it is alternatingly $+1$ and -1. In materials where only the nearest- and next-nearest-neighbor magnetic coupling is important, Eq. (9) can be solved to calculate the magnon frequencies.[5]

2. Inverse space formalism

The equations of motion can be further simplified by transforming to a normal-mode coordinate system. Owing to the underlying periodicity of the magnetic ground state, the normal modes are infinite-ranged plane-wave fluctuations with wave vector $\mathbf{q}$. To describe the periodicity, it is convenient to label atomic positions with a double index, one Greek letter labeling the atomic position inside the unit cell and the second defining the unit cell itself [shown schematically in Fig. (2)]:

$$\mathbf{R}_j = \mathbf{R}_{n+\mu} = \mathbf{T}_n + \vec{\tau}_{\mu}. \tag{11}$$

The magnitude of the moment M_j and the angle θ_j are the same in every unit cell, hence

$$M_j = M_{n+\mu} = M_{\mu} \quad \text{and} \quad \theta_j = \theta_{n+\mu} = \theta_{\mu}. \tag{12}$$

The periodicity of $\phi_i^{\mathbf{q}}(t)$ in Eq. (5) is given by the spin-spiral vector $\mathbf{q}$, which fulfills the relation

$$\phi_j^{\mathbf{q}}(t) = \phi_{n+\mu}^{\mathbf{q}}(t) = \mathbf{q}\cdot\mathbf{R}_{n+\mu} + \omega t. \tag{13}$$

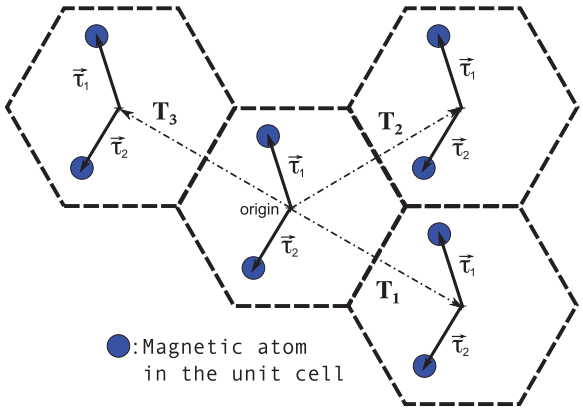

FIG. 2. (Color online) Example of the double index notation, where we have two magnetic atoms (located at $\vec{\tau}_1$ and $\vec{\tau}_2$) per unit cell (dashed hexagon).

By inserting Eqs. (13) and (12) in Eq. (6), we obtain the moment adapted to the symmetry shown in Fig. (1):

$$\mathbf{M}^{\mathbf{q}}_{n\mu}(t) = M_\mu \begin{pmatrix} \cos(\mathbf{q}\cdot\mathbf{R}_{n+\mu} + \omega t)\sin\theta_\mu \\ \sin(\mathbf{q}\cdot\mathbf{R}_{n+\mu} + \omega t)\sin\theta_\mu \\ \cos\theta_\mu \end{pmatrix}. \tag{14}$$

Thus Eq. (9) for the magnon modes transforms to

$$\begin{aligned}\theta^0_\mu \omega_{\mathbf{q}} &= \sum_\nu \sum_n J_{\nu+n\mu} M_{\nu+n}(1-\delta_{0n}\delta_{\mu\nu}) \\ &\quad\times\left[\theta^0_\mu - \theta^0_{\nu+n} A_\mu A_{\nu+n}\mathrm{Re}(\mathrm{e}^{-\mathrm{i}\mathbf{q}(\mathbf{R}_{n+\nu}-\mathbf{R}_\mu)})\right] \\ &= \sum_\nu \sum_n J_{\mu\nu+n} M_\nu(1-\delta_{0n}\delta_{\mu\nu}) \\ &\quad\times\left[\theta^0_\mu - \theta^0_\nu A_\mu A_\nu \mathrm{Re}(\mathrm{e}^{-\mathrm{i}\mathbf{q}(\mathbf{R}_{n+\nu}-\mathbf{R}_\mu)})\right],\end{aligned} \tag{15}$$

where the second step employs Eq. (12). The sum over n is merely the Fourier transform of the real-space coupling constants

$$J^{\mathbf{q}}_{\mu\nu} := -\sum_n (1-\delta_{0n}\delta_{\mu\nu}) J_{\mu,\nu+n}\mathrm{e}^{-\mathrm{i}\mathbf{q}(\mathbf{R}_{n+\nu}-\mathbf{R}_\mu)}. \tag{16}$$

Symmetry between the real-space coupling constants leads to the following relations:

$$J^{\mathbf{q}}_{\mu\nu} = J^{-\mathbf{q}}_{\nu\mu}, \quad \mathrm{Re}\left[J^{\mathbf{q}}_{\mu\nu}\right] = \mathrm{Re}\left[J^{\mathbf{q}}_{\nu\mu}\right], \tag{17}$$

$$\mathrm{Im}\left[J^{\mathbf{q}}_{\mu\nu}\right] = -\mathrm{Im}\left[J^{\mathbf{q}}_{\nu\mu}\right]. \tag{18}$$

In terms of the Fourier transformed coupling constants, the equation of motion then becomes

$$\theta^0_\mu \omega = \sum_\nu M_\nu \left(A_\mu A_\nu \mathrm{Re}\left[J^{\mathbf{q}}_{\mu\nu}\right] - \delta_{\mu\nu}\sum_\kappa \frac{M_\kappa}{M_\mu} J^{\mathbf{0}}_{\kappa\mu}\right)\theta^0_\nu, \tag{19}$$

$$\sqrt{M_\mu}\theta^0_\mu \omega = \sum_\nu \sqrt{M_\mu M_\nu}\mathrm{Re}\left[\tilde{J}^{\mathbf{q}}_{\mu\nu}\right]\sqrt{M_\nu}\theta^0_\nu \tag{20}$$

$$\Rightarrow 0 = \det\left(\delta_{\mu\nu}\omega_{\mathbf{q}} - \sqrt{M_\mu M_\nu}\mathrm{Re}\left[\tilde{J}^{\mathbf{q}}_{\mu\nu}\right]\right). \tag{21}$$

The magnon energies are thus the eigenvalues of the matrix $\sqrt{M_\mu M_\nu}\mathrm{Re}[\tilde{J}^{\mathbf{q}}_{\mu\nu}]$ with

$$\tilde{J}^{\mathbf{q}}_{\mu\nu} := A_\mu A_\nu J^{\mathbf{q}}_{\mu\nu} - \delta_{\mu\nu}\sum_\kappa \frac{M_\kappa}{M_\mu} J^{\mathbf{0}}_{\kappa\mu}. \tag{22}$$

Note that this result can be applied to FM or AFM ground states, as the prefactor A_μ in the definition of the $\tilde{J}^{\mathbf{q}}_{\mu\nu}$ is $+1$ for FM and alternatingly $+1$ and -1 for AFM.

3. *Magnon frequencies from DFT ground-state calculations*

In order to determine $\tilde{J}^{\mathbf{q}}_{\mu\nu}$ from DFT ground-state calculations, we start with writing the total energy per unit cell as

$$E_{\mathbf{q}} = E_0^{\mathrm{NM}} - \frac{1}{2N}\sum_{i\neq j} J_{ij}\mathbf{M}^{\mathbf{q}}_i(0)\cdot\mathbf{M}^{\mathbf{q}}_j(0), \tag{23}$$

where N is the total number of unit cells in the system and E_0^{NM} is the energy when the system is treated without magnetism. With Eq. (16) and the specific form of the moment [see Eq. (14)] the total energy in Eq. (23) reads

$$\begin{aligned}E_{\mathbf{q}} &= E_0^{\mathrm{NM}} + \frac{1}{2}\sum_{\mu\nu}^{\text{unit cell}} M_\mu M_\nu \\ &\quad\times\left(J^{\mathbf{0}}_{\mu\nu}\cos\theta_\mu\cos\theta_\nu + \sin\theta_\mu\sin\theta_\nu\mathrm{Re}\left[J^{\mathbf{q}}_{\mu\nu}\right]\right).\end{aligned} \tag{24}$$

For practical calculations, a spin spiral ansatz for the Kohn-Sham (KS) orbitals of the form $\varphi_{\mathbf{k}j}(\mathbf{r},\mathbf{q}) = \begin{pmatrix} u_{\mathbf{k}j,1}(\mathbf{r})e^{i(\mathbf{k}-\frac{\mathbf{q}}{2})\cdot\mathbf{r}} \\ u_{\mathbf{k}j,2}(\mathbf{r})e^{i(\mathbf{k}+\frac{\mathbf{q}}{2})\cdot\mathbf{r}}\end{pmatrix}$ is used to reproduce the moment in Eq. (14). Expanding $\sin\theta_\mu$ up to second order in the angle gives

$$\begin{aligned}E_{\mathbf{q}} &= \frac{1}{2}\sum_{\mu\nu} M_\mu M_\nu \left\{ J^{\mathbf{0}}_{\mu\nu}\left[1 - \frac{(\theta^0_\mu)^2}{2} - \frac{(\theta^0_\nu)^2}{2}\right]\right. \\ &\quad\left. + A_\mu A_\nu \mathrm{Re}\left[J^{\mathbf{q}}_{\mu\nu}\right]\theta^0_\mu\theta^0_\nu\right\} + E_0^{NM}.\end{aligned} \tag{25}$$

The second derivative of this energy with respect to the angle θ^0_μ leads to the needed coupling constant and the resulting equation reads

$$\mathrm{Re}\left[\tilde{J}^{\mathbf{q}}_{\mu\nu}\right] = \frac{1}{M_\mu M_\nu}\left.\frac{\partial^2 E_{\mathbf{q}}(\{\theta^0_\mu\})}{\partial\theta^0_\mu\partial\theta^0_\nu}\right|_{\{\theta^0_\mu\}=0}. \tag{26}$$

This provides a procedure to calculate magnon energies using DFT ground-state calculations: first the energy surfaces, $E_{\mathbf{q}}(\{\theta^0_\mu\})$, are determined by fully self-consistent ground-state calculations, then the second derivative of these energy surfaces is calculated to get the matrix elements $\mathrm{Re}[\tilde{J}^{\mathbf{q}}_{\mu\nu}]$, and finally, the diagonalization of the matrix $\sqrt{M_\mu M_\nu}\mathrm{Re}[\tilde{J}^{\mathbf{q}}_{\mu\nu}]$, is performed to obtain the magnon energies. The computationally most demanding part of this procedure is the calculation of the energy surface.

B. Magnons in the TMOs

To simplify the calculation of the energy surface, one can exploit the symmetry of the system under investigation. TMOs have two magnetic atoms per unit cell with equal (in magnitude) on-site moments and an AFM ordering which implies that $\theta_1 \approx 0$ and $\theta_2 \approx \pi$. Hence Eq. (21) for the magnon modes simply becomes

$$\sqrt{\left(\omega_{\mathbf{q}} - M\mathrm{Re}\left[\tilde{J}^{\mathbf{q}}_{11}\right]\right)\left(\omega_{\mathbf{q}} - M\mathrm{Re}\left[\tilde{J}^{\mathbf{q}}_{22}\right]\right)} = \pm M\mathrm{Re}\left[\tilde{J}^{\mathbf{q}}_{12}\right]. \tag{27}$$

Due to the symmetry of the crystal (see Fig. 2) and the transformation defined in Eq. (16), the following symmetry relations can be obtained:

$$J_{12}^{\mathbf{q}+\mathbf{b}_3} = -A_1 A_2 \sum_k J_{1,2+k} e^{-i(\mathbf{q}+\mathbf{b}_3)(\vec{\tau}_2 - \mathbf{R}_k - \vec{\tau}_1)} = -J_{12}^{\mathbf{q}} \quad (28)$$

$$J_{\mu\mu}^{\mathbf{q}+\mathbf{b}_3} = J_{\mu\mu}^{\mathbf{q}}. \quad (29)$$

These symmetry relations and Eq. (27), then lead to $\pm\mathrm{Re}[\tilde{J}_{12}^{\mathbf{q}}] = \mp\mathrm{Re}[\tilde{J}_{12}^{\mathbf{q}}] = 0$. Thus the two magnon modes given in Eq. (27) are

$$\omega_{\mathbf{q}1} = M\mathrm{Re}\big[\tilde{J}_{11}^{\mathbf{q}}\big] \quad \text{and} \quad \omega_{\mathbf{q}2} = M\mathrm{Re}\big[\tilde{J}_{22}^{\mathbf{q}}\big]. \quad (30)$$

The symmetry of the problem thus reduces the number of needed matrix elements in Eq. (21) from four to two. It is further possible to lower the computational cost by determining the magnon energies without calculating the derivative of the full energy surface as implied by Eq. (26). This can be achieved by exploiting the symmetry relation $J_{\mu\nu}^{\mathbf{q}} = \delta_{\mu\nu} J_{\mu\mu}^{\mathbf{q}}$ that leads to the following simplification of Eq. (25):

$$E_{\mathbf{q}} = E_0^{\mathrm{NM}} + \frac{M^2}{2} \sum_{\mu=1}^{2} \left\{ J_{\mu\mu}^{\mathbf{0}} \left[1 - \left(\theta_\mu^0\right)^2\right] \mathrm{Re}\left(J_{\mu\mu}^{\mathbf{q}}\right) \left(\theta_\mu^0\right)^2 \right\} \quad (31)$$

$$= E_0^{\mathrm{NM}} + \frac{M^2}{2} \sum_{\mu=1}^{2} \left[J_{\mu\mu}^{\mathbf{0}} + \mathrm{Re}\left(\tilde{J}_{\mu\mu}^{\mathbf{q}}\right) \left(\theta_\mu^0\right)^2 \right]. \quad (32)$$

In this equation, the first term is the nonmagnetic energy, the second term is the magnetization energy ($E_0^{\mathrm{AFM}} - E_0^{\mathrm{NM}}$), and the last term is the energy contribution from the spin spiral. Since the two magnetic atoms are equivalent [see Fig. 3], Eq. (32) can be further rewritten as

$$\frac{2\left(E_{\mathbf{q}} - E_0^{\mathrm{AFM}}\right)}{M^2} = \mathrm{Re}\left(\tilde{J}_{11}^{\mathbf{q}}\right)\left[\left(\theta_1^0\right)^2 + \left(\theta_2^0\right)^2\right]. \quad (33)$$

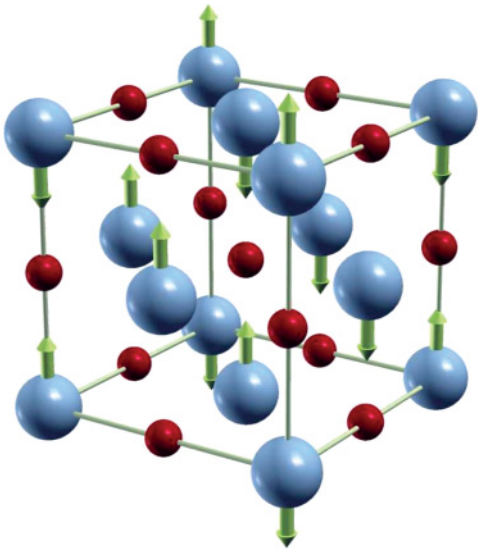

FIG. 3. (Color online) AFM structure of the TMOs; the red balls are oxygen and the large blue ones are the TM atoms. The yellow arrows indicate the localized magnetic moments.

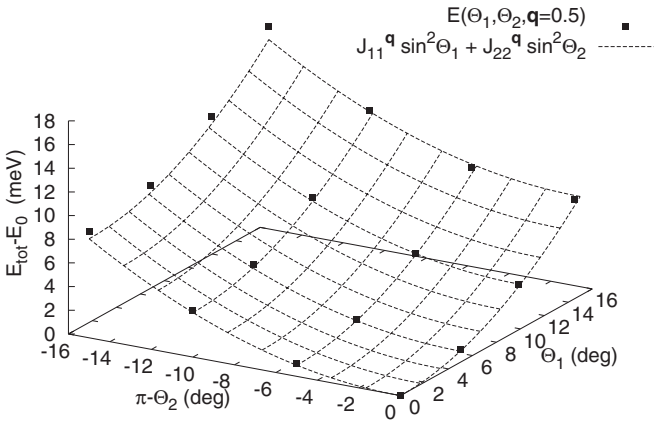

FIG. 4. The energy surface $E_{\mathbf{q}} - E_0^{\mathrm{AFM}}$ as a function of the angles θ_1 and θ_2 for NiO. The energies have been calculated with LSDA using $\mathbf{q} = \mathbf{b}_3/2$.

To solve Eq. (33), one can set

$$\theta_1 = \theta_1^0 = \theta \quad \text{and} \quad \theta_2 - \pi = \theta_2^0 = \theta.$$

Inserting this in Eq. (33) and using Eq. (30) leads to the final expression for magnon frequencies:

$$\omega_{\mathbf{q}} = \frac{\left[E_{\mathbf{q}}(\theta, \pi + \theta) - E_0^{\mathrm{AFM}}\right]}{M\theta^2}. \quad (34)$$

For practical calculations, one still needs to choose a value for the angle θ. This choice is not easy since, in principle, this angle needs to be infinitesimal. However, moderately large values of θ can be used. In Fig. 4, the energy surface $E_{\mathbf{q}} - E_0^{\mathrm{AFM}}$ as a function of the angles θ_1 and θ_2 is shown. Good agreement between the analytic solution [see Eq. (33)] and the calculated values show that Eq. (34) is valid up to an angle of $\sim 15^\circ$.

C. The Néel Temperature

The Néel temperature T_N is the temperature where the long-range AFM order is lost and the system becomes paramagnetic (PM). The thermal average (depicted with $\langle\rangle_T$) of the on-site moment within mean field approximation (MFA) is

$$\langle M_{\nu,}\rangle_T = M_\nu \coth\left(\frac{A_\nu M_\nu B_\nu^{\mathrm{eff}}}{\mathrm{k}_B T}\right) - \frac{1}{\beta B_\nu^{\mathrm{eff}}}, \quad (35)$$

where the effective magnetic field is defined as

$$B_\mu^{\mathrm{eff}} := \sum_\nu^{\text{unit cell}} A_\nu J_{\mu\nu}^{\mathbf{0}} \langle M_\nu \rangle_T. \quad (36)$$

Close to the critical temperature the effective field vanishes and $\coth(x)$ can be expanded and the lowest order term gives

$$\det\left[T\delta_{\mu\nu} - \frac{A_\mu A_\nu M_\mu^2 J_{\mu\nu}^{\mathbf{0}}}{3\mathrm{k}_B}\right] = 0, \quad (37)$$

where the smallest eigenvalue of T gives the Néel temperature. In the case of the TMOs, we only have diagonal terms and $J_{11}^{\mathbf{0}} = J_{22}^{\mathbf{0}}$, hence the solution simplifies to the well-known expression

$$\mathrm{k}_B T_N^{\mathrm{MFA}} = \frac{M^2 J_{11}^{\mathbf{0}}}{3}, \quad (38)$$

where the thermal energy required to destroy the long-range AFM order depends only on $J_{11}^{\mathbf{0}}$. The $J_{11}^{\mathbf{0}}$ can be obtained by integrating Eq. (22) over the Brillouin zone (BZ):

$$\int_{\mathrm{BZ}} d^3q\ \tilde{J}_{11}^{\mathbf{q}} = \int_{\mathrm{BZ}} d^3q \sum_{n\neq 0} J_{1,1+n}(1-e^{-i\mathbf{q}\cdot\mathbf{T}_n})$$
$$= V_{\mathrm{BZ}} J_{11}^{\mathbf{0}} - \sum_{n\neq 0} J_{1,1+n} \underbrace{\int_{\mathrm{BZ}} d^3q e^{-i\mathbf{q}\cdot\mathbf{T}_n}}_{=0 \text{ because } \mathbf{T}_n\neq\mathbf{0}}$$
$$\Rightarrow J_{11}^{\mathbf{0}} = \frac{1}{V_{\mathrm{BZ}}}\int_{\mathrm{BZ}} d^3q\ \tilde{J}_{11}^{\mathbf{q}} = \frac{1}{V_{\mathrm{BZ}}M}\int_{\mathrm{BZ}} d^3q\ \omega_{\mathbf{q}}.$$

Finally, the expression for the T_N in MFA becomes (using a discreet set of $\mathbf{q}$ points)

$$\mathrm{k}_B T_N^{\mathrm{MFA}} = \frac{M}{3}\left[\frac{1}{N}\sum_{\mathbf{q}=\mathbf{0}}^{\mathrm{BZ}} \omega_{\mathbf{q}}\right], \tag{39}$$

where N is the number of calculated magnon energies. Another way of calculating the Néel temperature is by using the random phase approximation (RPA),[35]

$$\mathrm{k}_B T_N^{\mathrm{RPA}} = \frac{MN}{3}\left[\sum_{\mathbf{q}\neq\mathbf{0}}^{\mathrm{BZ}} \frac{1}{\omega_{\mathbf{q}}}\right]^{-1}. \tag{40}$$

Note, that the only difference between Eqs. (39) and (40) is the kind of average performed. In the harmonic average used for the RPA, small values have a strong weight, and therefore the statement

$$T_N^{\mathrm{RPA}} < T_N^{\mathrm{MFA}}$$

can be shown to be true.[36]

III. COMPUTATIONAL DETAILS

All calculations are performed using the state-of-the-art full-potential linearized augmented plane-wave (FPLAPW) method,[37] as implemented within the ELK code.[38] To obtain the Pauli spinor states, the Hamiltonian containing only the scalar potential is diagonalized in the LAPW basis: this is the first-variational step. The scalar states thus obtained are then used as a basis to set up a second-variational Hamiltonian with spinor degrees of freedom.[37] This is more efficient than simply using spinor LAPW functions, but care must be taken to ensure that there is a sufficient number of first-variational eigenstates for convergence of the second-variational problem.

For the lattice constants, we use the experimental values[39] and neglect the small rhombohedral or tetragonal distortions.[40,41] We have used a total of 330 $\mathbf{k}$ points in the irreducible BZ and 100 states per $\mathbf{k}$ point. This ensures convergence of the second-variational step. The potential and density are expanded with a plane-wave cutoff of $|\mathbf{G}| = 14/a_0$, additionally $R_{\mathrm{min}} \times |\mathbf{G}+\mathbf{k}|$ is limited to 8.5, where R_{min} is the smallest muffin-tin (MT) radius in the system. The MT radii in a.u. are NiO = (2.024; 1.725), CoO = (2.026; 1.767), FeO = (2.078; 1.791), and MnO = (2.137; 1.852) for the transition metal and oxygen, respectively. The maximum l for the expansion of the wave function inside the MT is eight and a smearing width of 1 mHa is used.

Calculations are performed using the GGA $+U$ and LSDA $+U$ functional within DFT. For the Hubbard term in Eq. (A1), we used the most general version, which contains two independent parameters U and J.[13] Unless otherwise mentioned, we always use the fully localized limit (FLL) for the double-counting term.[14] For the LSDA functional, we used the Perdew-Wang parametrization[42] and for GGA, the Perdew, Burke, and Ernzerhof[43] functional is used.

For the magnon calculation, the moments have to make a small angle with the z axis and this is achieved by applying a small magnetic field in the MT sphere. The fields have a magnitude of less than 10^{-3} a.u. and are used to fix only the direction of the moment, the magnitude, on the other hand, is fully self-consistently obtained. For the present calculations, we use an angle of $\theta = 15^\circ$, which is a reasonable choice [see Fig. 4]. For calculating the critical temperatures, a $\mathbf{q}$ grid of $3\times3\times2$ points is used.

IV. RESULTS

A. Gap and moment

There are several ways of estimating the value of U; the original idea was to choose the value of U based on constrained LSDA calculations.[9] Later, another scheme based on the linear response was proposed.[16] These two methods keep the LSDA $+U$ scheme *ab initio* in nature. However, to reduce the computational cost, in many calculations, the value of U has been chosen to reproduce one of the experimental observables like gap, moment,[12,44,45] density of states (DOS),[6,15,24] etc. As a consequence of this, widely different values of U are used for the same material; for example, in the case of NiO, the value of the on-site repulsion ranges from 4.6 to 8 eV depending upon the method.[9,16] In order to gain insight into how the choice of U affects the ground-state properties of the TMOs, we analyze in this section, the behavior of the gap and the on-site magnetic moment as a function of U. These ground-state properties, especially the on-site moment, are important for calculating the magnon spectrum of the system [see Eq. (30)], determination of which is one of the main aims of this work.

The gaps for NiO, CoO, FeO, and MnO as functions of U obtained using LSDA $+U$ and GGA $+U$ are shown in Fig. 5. At this point, it is important to mention that, unlike for other TMOs, FeO has a metallic ground state even when treated with LSDA $+U$. In order to obtain a gap for FeO, an explicit symmetry breaking by inclusion of an $\mathbf{L}\cdot\mathbf{S}$ term in the Hamiltonian is required.

For small (0–4 eV) and intermediate (4–6 eV) values of U the gap increases linearly. This behavior can be understood by looking at Eq. (A17). Occupied d states are shifted down in energy whereas d states above the Fermi energy are shifted up. The shift is proportional to U so the gap starts to increase linearly. These results are similar to the previous results of Petukhov *et al.*[14] For large values of U (6–12eV), the d states are shifted beyond states with mainly oxygen p character. Since these states are only weakly affected by the LSDA $+U$ Hamiltonian (see discussion in Appendix), the gap starts to saturate.

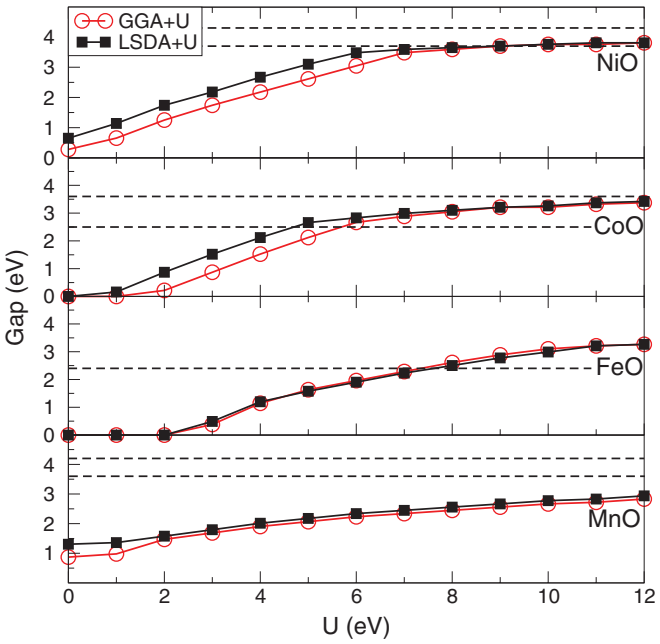

FIG. 5. (Color online) Gap (in eV) as a function of U (in eV). The closed symbols are LSDA + U, the open ones are GGA + U and the dashed lines indicate the range of reported experimental values for the gap.

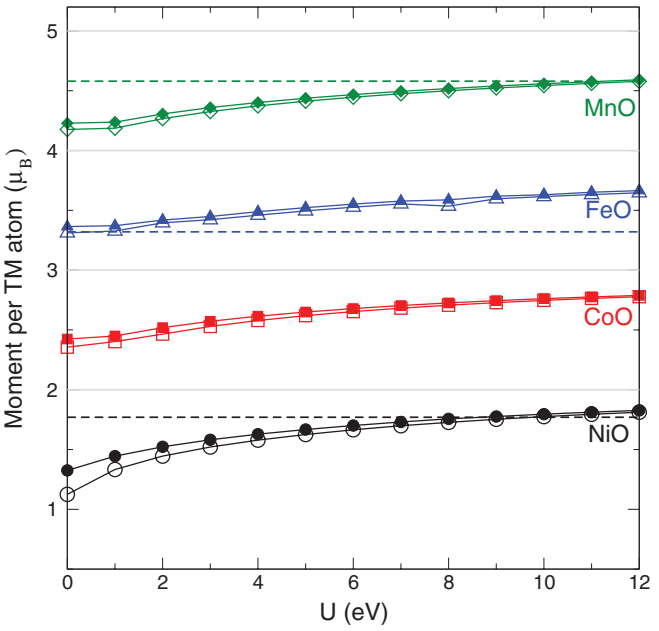

FIG. 6. (Color online) Moment (in μ_B) as a function of U (in eV). The closed symbols are LSDA + U, the open ones are GGA + U, the dashed lines are the experimental values[40,56,57] for the moment and the solid gray lines are the pure spin limits.

The measured gap varies for each material depending on the used experimental technique. The reported values for the gaps are $\Delta_{\mathrm{NiO}} = 3.7$–$4.3$ eV,[46,47] $\Delta_{\mathrm{CoO}} = 2.5$–$3.6$ eV,[48,49] $\Delta_{\mathrm{FeO}} = 2.4$ eV,[50] and $\Delta_{\mathrm{MnO}} = 3.6$–$4.2$ eV.[51–53] For NiO, CoO, and FeO, a reasonably good agreement between experiment and the calculated gaps (with intermediate values of U) is found. For MnO, on the other hand, the gap is always underestimated compared to the experimental values. Even for very large values of $U > 30$ eV, the calculated gap does not reach the experimental value. However, it has been shown that the experimental gap can be reproduced by taking many-body corrections on the level of a GW calculation into account.[54,55]

In Fig. 6, the on-site magnetic moments $|\mathbf{M}_I|$ as functions of U are presented. The moment is given by

$$|\mathbf{M}_I| = \sum_{m=-2}^{2} \left(n_{mm}^{I\uparrow} - n_{mm}^{I\downarrow}\right) = N_I^{\uparrow} - N_I^{\downarrow},$$

where the orbital occupation numbers $n_{mm}^{I\sigma}$ of d states at lattice site I are defined in Eq. (A4). The limit $N_I^{\uparrow} = 5$ and $N_I^{\downarrow} = \{3,2,1,\text{ or } 0\}$, for Ni, Co, Fe, and Mn, respectively, is the "pure spin limit.' For any physical value of U, the pure spin limit sets the least upper bound for $|\mathbf{M}_I|$.

For $U = 0$, the orbitals with spin up are filled to approximately 90%($N_I^{\uparrow} \approx 4.5$) and the occupation of the down spin states is about 10% above the minimal vales of $\{3,2,1,\text{ or } 0\}$. Hence, the value of the moment is $\approx 0.7\ \mu_B$ below the pure spin limit. On increasing the on-site repulsion, the occupation numbers change. States with $n_{mm}^{I\sigma} > 0.5$ are shifted down in energy and states with $n_{mm}^{I\sigma} < 0.5$ are shifted up. The magnitude of the energy shift is proportional to U (see discussion in part 4 of Appendix). The energy shift changes the occupation numbers toward the pure spin limit. The more the states are shifted (larger U), the closer the system gets to the pure spin limit. Hence, the moments increase with increasing U. The enhancement of the moment induced by $U = 12$ eV is almost the same in all TMOs. The largest increase is observed in NiO ($\approx 0.5\ \mu_B$) and the smallest one in FeO ($\approx 0.3\ \mu_B$).

The moments calculated with intermediate values of U (4–6eV) for NiO, FeO, and MnO are in agreement with the experimental data (with a maximum error of 8% for MnO). The experimental value of the moment for MnO ($4.58\ \mu_B$)[40] is reached only for very large values of U, while for FeO, even with $U = 0$, a good agreement with experiments can be obtained. For CoO, all reported experimental data are above the pure spin limit of $3\mu_B$ due to large contributions from orbital-angular momentum.[41,56–58] Finally, we note that for $U \gtrsim 6$ eV, LSDA + U and GGA + U lead to the same values for the gap and the moment.

B. Remark on FeO

For FeO, the LSDA + U method does not open a gap without including spin-orbit ($\mathbf{L}\cdot\mathbf{S}$) coupling. After this symmetry breaking, we get a reasonable gap for FeO. This inclusion of spin-orbit coupling has dire consequences; to calculate the magnon spectrum, the following ansatz for the Kohn-Sham orbitals is used:

$$\varphi_{\mathbf{k}j}(\mathbf{r},\mathbf{q}) = \underbrace{\begin{pmatrix} e^{i\left(\mathbf{k}-\frac{\mathbf{q}}{2}\right)\cdot\mathbf{r}} & 0 \\ 0 & e^{i\left(\mathbf{k}+\frac{\mathbf{q}}{2}\right)\cdot\mathbf{r}} \end{pmatrix}}_{=\overleftrightarrow{A}} \begin{pmatrix} u_{\mathbf{k}j,1}(\mathbf{r}) \\ u_{\mathbf{k}j,2}(\mathbf{r}) \end{pmatrix},$$

where the functions $u_{\mathbf{k}j,1}$ fulfill the boundary condition $u_{\mathbf{k}j,1}(\mathbf{r}) = u_{\mathbf{k}j,1}(\mathbf{r}+\mathbf{R})$. This ansatz is chosen in such a way that only the chemical unit cell is required to calculate the spin-spiral energy for any value of the spin-spiral vector

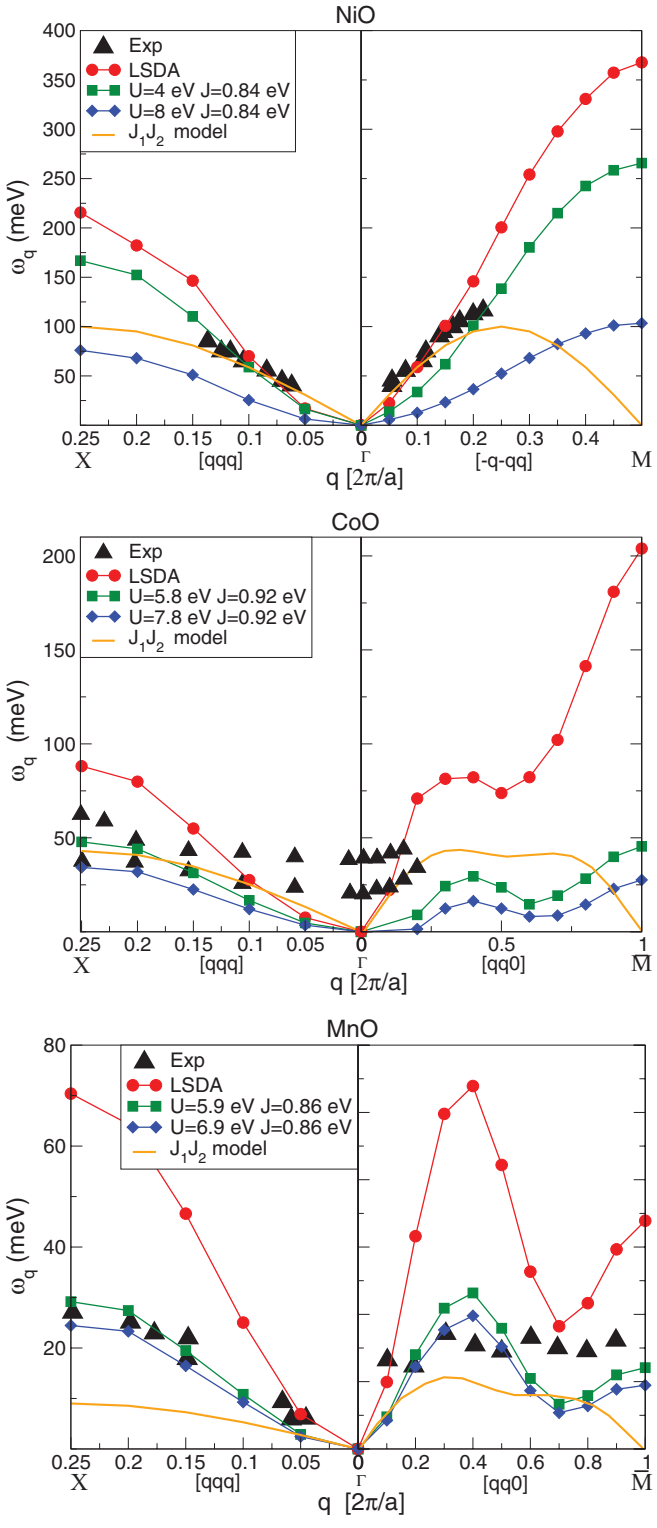

FIG. 7. (Color online) Magnon spectrum for NiO, CoO, and MnO. LSDA results are shown with red circles, the two different values of U with green squares and blue diamonds, experiment[61–63] with black triangles, and the $J_1 J_2$ results[5] with orange line.

q. Since the larger magnetic unit cells are not needed, the calculation can be performed even for very small values of **q** (long-range excitation), which are required to determine the magnon spectrum.[59] The condition for this "unwinding" process is

$$[V_{\mathrm{KS}}, \overleftrightarrow{A}]_- = 0,$$

where V_{KS} is the 2×2 potential in the KS equations. If the $\mathbf{L} \cdot \mathbf{S}$ term is added to the KS potential, the commutator relation is not fulfilled anymore and a calculation of magnons with this technique is not possible.

C. Magnon spectra

As shown in the above section, using the LSDA + U method with an intermediate value of U, the moments (gaps) for TMOs are reproduced to within 8% (44%) in the worst case. The question then arises how well is the magnon spectrum reproduced within the LSDA + U technique. The calculation of the magnon spectrum is challenging as it sensitively relies not just on the ground-state magnetic moment but also on the interatomic magnetic interactions, reproduction of which has proved to be a difficult task for strongly correlated materials.[60]

The magnon spectrum obtained using LSDA and LSDA + U with two different values of U are presented together with experimental data in Fig. 7. It is interesting to note that in the small-$|\mathbf{q}|$ limit, i.e., close to the Γ point, LSDA magnon frequencies are in good agreement with the experimental data. As one goes away from the zone center, the LSDA functional overestimates the magnon frequencies. Switching on the Coulomb repulsion U, improves these overestimated magnon energies. Increasing U has a dramatic effect on the magnon energies; for example, in the case of NiO at the M point, the magnon energy changes by 160% on changing the value of U from 4 to 8 eV.

In order to see how the long-range magnetic interactions affect the magnon spectrum for TMOs, we also compare our findings with the standard nearest- and next-nearest-neighbor ($J_1 J_2$) model[5] (depicted with the cyan curve in Fig. 7). We find a striking difference between the present calculation and the $J_1 J_2$ model; finite energies at the special points M and $\bar{\mathrm{M}}$ in agreement with experiment are obtained on the use of long-range magnetic interactions, while the use of nearest- and next-nearest-neighbor interactions in the $J_1 J_2$ model incorrectly leads to vanishing magnon energies at M and $\bar{M}$. We also note that the linear behavior close to the Γ point found in the $J_1 J_2$ model is not obtained in the present case. This discrepancy is due to the well-known sensitivity of the magnon energies in the small-**q** limit (negative magnon energies for CoO close to the Γ point). The experimental magnon spectrum in CoO shows finite energies at the Γ point [in contradiction with Eq. (34)] and a splitting of the two magnon modes. Both effects can be captured by extending the Heisenberg model in Eq. (1) by an $\mathbf{L} \cdot \mathbf{S}$ and an $\mathbf{L}^2$ term.[61] But these terms would break the spin-wave symmetry as discussed in Sec. IV B and make a calculation of the magnon spectrum impossible. In order to gain insight into the behavior of the magnon spectrum as a function of U (i.e., strong suppression of the magnon frequencies), it is instructive to look at the change in charge distribution around the constituent atoms within the unit cell. This analysis is performed in the following section.

D. Charge distribution

In this section, we present the spatially averaged charge on TM and oxygen atoms calculated using various values of U. In order to make a systematic comparison between all TMOs, it is convenient to introduce a parameter λ, such that

$$U = \lambda U_0 \quad \text{and} \quad J = \lambda J_0. \tag{41}$$

where U_0 and J_0 are the material specific screened averaged Coulomb repulsion obtained using the constrained LSDA method and $\lambda = 0$ is the pure LSDA limit. [The constrained LSDA results[9] for the TMOs for $(U; J)$ in eV are $(8.0; 0.95)_{\mathrm{NiO}}$, $(7.8; 0.92)_{\mathrm{CoO}}$, $(6.8; 0.89)_{\mathrm{FeO}}$, and $(6.9; 0.86)_{\mathrm{MnO}}$]. In Fig. 8, we plot the difference between $N_{\mathrm{LDA+U}}$ and N_{LDA} as a function of λ, where the $N_{\mathrm{LDA+U}}$ and N_{LDA} are the MT or interstitial charge, respectively:

$$N_{\mathrm{LDA}} = \int_V d^3\mathbf{r}\, \rho_{\mathrm{LDA}}(\mathbf{r}) \quad \text{with } V = \begin{cases} \text{muffin tin,} \\ \text{interstitial region.} \end{cases}$$

For all materials, a qualitatively similar behavior is observed; by increasing λ, charge accumulates in the oxygen MT and depletes from the transition-metal and the interstitial region. This behavior is a direct consequence of the on-site repulsion U acting on the TM d states, which pushes the charge away from the TM atom. The effect of U is strongest for Ni and decreases down the series being weakest for the Mn atom. As expected, the reduction in the charge of the interstitial region as a function of λ indicates an increased localization of electrons due to increasing Coulomb repulsion. On the basis of this behavior of the charge, it is easy to explain the trend in the magnon spectrum as a function of U; the magnon energy is proportional to the on-site moment and the magnetic coupling constant [see Eq. (30)]. The change in moment as a function of U is quite small (the maximum change in moment is for MnO by 8% on going from $U = 4$ to 8 eV), hence the dominating term that leads to the suppression of the magnon energies as a function of U is the magnetic coupling constant, which is reduced by the enhanced charge localization.

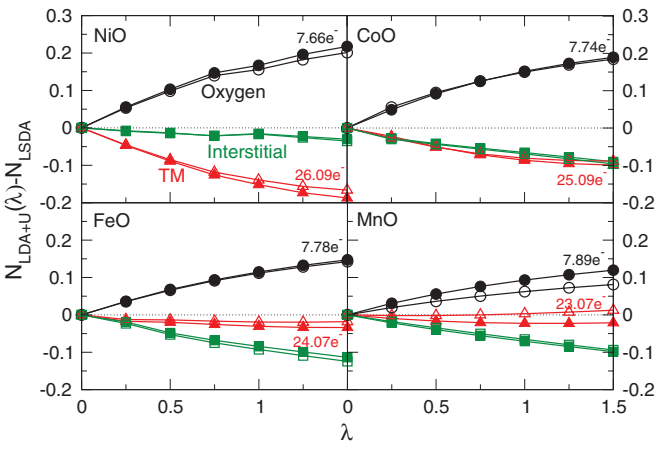

FIG. 8. (Color online) Amount of charge located in the atom muffin tin as a function of the parameter λ [see Eq. (41)]. Plotted are always the differences to $\lambda = 0$ values. The open symbols are GGA + U, the filled are LSDA + U calculations. For all materials, the TM charge is plotted with red triangles, oxygen with black circles, and the interstitial region with green squares. The numbers at the right upper and lower corners denote the number of electrons in the muffin tin for the maximum value of λ.

At this point it is also worth mentioning that the charge calculated using the LSDA ($\lambda = 0$) shows the correct trend; NiO is the most electronegative and MnO is the least with $\mathrm{Ni}^{+1.72}$, $\mathrm{Co}^{+1.81}$, $\mathrm{Fe}^{+1.89}$, and $\mathrm{Mn}^{+1.91}$. However, for large values of λ (above $\approx$1.2), all the TM atoms have almost the same electronegativity contrary to physical reality.

E. Néel Temperatures

Given the magnon energies using Eq. (34), the Néel temperature can be easily determined. The calculated Néel temperatures for various values of U are shown in Fig. 9. These results are obtained using two different approximations for averaging the magnon frequency; mean-field approximation (MFA) [see Eq. (39)] and the random phase approximation (RPA) [see Eq. (40)]. As expected from the behavior of the magnon energies (see Sec. IV C), the critical temperature decreases as the value of U increases. For comparison, in Fig. 9, the experimental data are shown as dashed line. It is well known that the MFA overestimates the Néel temperatures. Hence, for larger values of U, where the magnon energies are suppressed due to charge localization, the Néel temperatures calculated using MFA are in reasonable agreement with the experimental data. The RPA, on the other hand, is well known to underestimate the Néel temperature. This can also be seen in Fig. 9. This means that intermediate values of U lead to reasonable agreement with the experimental data in this case. At this point, it is important to note that the magnon energies for MnO are very small as compared to other TMOs, which makes the harmonic averaging of magnon energies, required by the RPA, very sensitive, leading to Néel temperatures well below the experimental data.

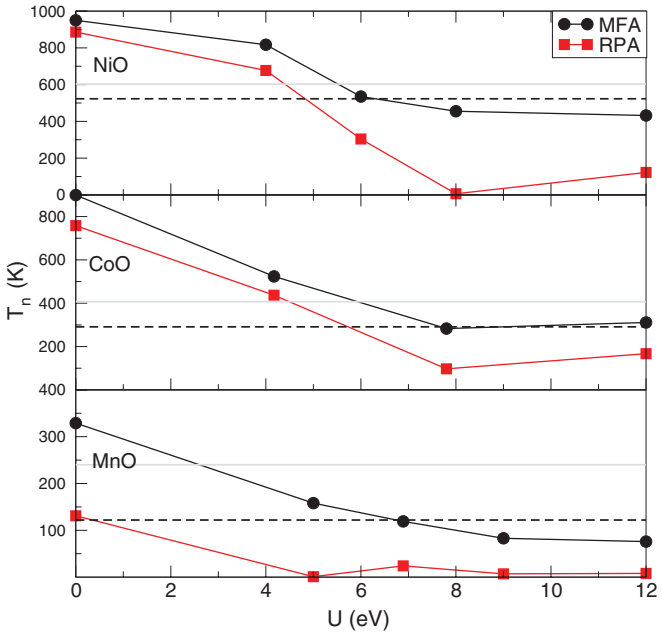

FIG. 9. (Color online) Néel temperatures as a function of U for NiO, CoO, and MnO. The dashed lines denote the experimental values[56] and the gray solid lines are Monte Carlo simulations.[29]

V. SUMMARY

We have determined the magnon frequencies for TMOs using the frozen magnon approach combined with the LSDA + U formalism. The value of U is systematically increased to investigate the effect of the on-site Coulomb repulsion on various ground-state properties and the magnon frequencies. A brief overview of the general formalism for treating magnons, including an infinite number of magnetic interactions is presented in the first part of the paper.

In the second part of the paper, we present results for the gap and the on-site moment as a function of U. The qualitative behavior of the gap and moment as a function of U is the same for the materials under investigation. The experimental results are well reproduced for intermediate values of U with two exceptions: (1) the magnetic moment of CoO and (2) the gap of MnO. The discrepancies are explained by an orbital-angular momentum and many-body effects, respectively.

In the third part, we have presented the calculated magnon spectrum for various values of U. The magnon energies are strongly suppressed on increasing the on-site Coulomb repulsion. The reason for this behavior is pinned to charge localization: the magnon energies are proportional to the on-site moment and the intersite magnetic coupling constant. The on-site moment depends weakly on the Coulomb repulsion but the magnetic coupling constant shows a very strong dependence on U. We demonstrate by analyzing the spatially averaged charge that this strong dependence of the intersite magnetic interactions on U is a direct consequence of the strong charge localization.

We compare our approach for calculating magnon energies, which includes magnetic interactions between infinite number of neighbors, with the standard (nearest-) next-nearest-neighbor $J_1 J_2$ model. This comparison highlights the importance of including long-range interactions especially to correctly find finite magnon energies at the zone boundary.

Since the Néel temperature in MFA or RPA is found by averaging magnon energies, the U dependence of T_N is similar to the U dependence of the magnon energies. For values of U between 5–8 eV, the MFA as well as the RPA reproduce the experimental Néel temperature.

The proper choice of the parameter U is critical, especially for the sensitive properties (gap and magnons). We have found for the gap, moment, charge, magnon spectrum, and T_N^{RPA} a reasonably good agreement with experiment, for intermediate values of U (ranging from 4 to 6 eV) for the TMOs under investigation in the present work.

APPENDIX: LSDA + U METHOD

Despite the success of the LSDA, it fails to describe Mott insulators. On the other hand, the LSDA + U method has proved to be able to reproduce the correct band structure for the Mott insulators.[9] These materials have a partially filled d (or f) shell and a d-d (or f-f) band gap. The gap is caused by a large on-site Coulomb repulsion, which splits the d (or f) bands in a lower (occupied) and upper (unoccupied) Hubbard bands.

In order to derive the LSDA + U total energy, one starts from the Hartree-Fock (HF) approximation. It leads to a general orbital-dependent form of the exchange interaction (it contains no correlation), also known as the Fock term. The orbitals in the Fock term are expanded in terms of an atomic-basis set, followed by this, the atomic Slater integrals occurring in HF are replaced by effective screened integrals, expressed in terms of two parameters U^I and J^I.[64] This screened HF term, E^{HF}, is reminiscent of a Hubbard-like term and when combined together with the conventional LSDA formalism is termed as the LSDA + U method.

1. The LSDA + U total energy

The total energy of the LSDA + U method consists of the LSDA total energy plus a HF term. [Instead of the LSDA total energy, the generalized gradient approximation (GGA) can also be used. In this case, the method is called GGA + U.] Since the interactions contained in E^{HF} are also partially included in E^{LSDA}, a double-counting (DC) term E^{DC} needs to be subtracted from the total energy functional:[13,64,65]

$$E^{\mathrm{LSDA}+U} = E^{\mathrm{LSDA}}[\rho] + \underbrace{E^{\mathrm{HF}} - E^{\mathrm{DC}}}_{:=E^{\mathrm{U}}} = E^{\mathrm{LSDA}} + E^{\mathrm{U}}. \quad \text{(A1)}$$

The term E^{HF} can be derived directly from the orbital-dependent interaction energy in the HF scheme. In terms of the occupied single-particle Kohn-Sham orbitals, the direct Coulomb term is

$$E^{\mathrm{H}} = \frac{1}{2}\sum_{ij}^{\mathrm{occ}} \langle \varphi_i \varphi_j | \hat{v} | \varphi_i \varphi_j \rangle, \quad \text{(A2)}$$

and the exchange term is

$$E^{\mathrm{F}} = -\frac{1}{2}\sum_{ij}^{\mathrm{occ}} \langle \varphi_i \varphi_j | \hat{v} | \varphi_j \varphi_i \rangle. \quad \text{(A3)}$$

These integrals for localized d and f electrons can be isolated by expanding the Kohn-Sham orbitals in terms of a localized atomic basis $|I,nlm\sigma\rangle$. I denotes the lattice site, n is the main quantum number, l is the orbital quantum number, m is the magnetic quantum number, and σ is the spin index. The direct Coulomb term then looks like

$$E^{\mathrm{H}} = \frac{1}{2}\sum_{I}\sum_{ij}^{\mathrm{occ}}\sum_{\{\sigma_i m_i\}} \delta_{\sigma_1\sigma_3}\delta_{\sigma_2\sigma_4} \langle \varphi_i \varphi_j | I, m_1\sigma_1 m_2\sigma_2 \rangle \times \underbrace{\langle I, m_1 m_2 | \hat{v} | I, m_3 m_4 \rangle}_{:=M^I_{m_1 m_2 m_3 m_4}} \langle I, m_3\sigma_3 m_4\sigma_4 | \varphi_i \varphi_j \rangle.$$

The occupation number matrix elements of one lattice site can now be introduced:

$$n^{I\sigma}_{mm'} := \sum_{i}^{\mathrm{occ}} \langle \varphi_i | I, m\sigma \rangle \langle I, m'\sigma | \varphi_i \rangle. \quad \text{(A4)}$$

In terms of these occupation numbers, the direct Coulomb term reads

$$E^{\mathrm{H}} = \frac{1}{2}\sum_{I}\sum_{\sigma\sigma'}\sum_{\{m_i\}} n^{I\sigma}_{m_1 m_3} n^{I\sigma'}_{m_2 m_4} M^I_{m_1 m_2 m_3 m_4}. \quad \text{(A5)}$$

The same procedure can be performed for the exchange term, which leads to

$$E^{\mathrm{F}} = -\frac{1}{2}\sum_{I}\sum_{\sigma}\sum_{\{m_i\}} n^{I\sigma}_{m_1m_3} n^{I\sigma}_{m_2m_4} M^{I}_{m_1m_2m_4m_3}. \tag{A6}$$

We collect the Coulomb term [see Eq. (A5)] and the exchange term [see Eq. (A6)], which results in the screened correction to the LSDA energy in Eq. (A1):

$$E^{\mathrm{HF}} = \frac{1}{2}\sum_{I}\sum_{\sigma}\sum_{\{m_i\}}\Big[n^{I\sigma}_{m_1m_3} n^{I-\sigma}_{m_2m_4} M^{I}_{m_1m_2m_3m_4} - n^{I\sigma}_{m_1m_3} n^{I\sigma}_{m_2m_4}\big(M^{I}_{m_1m_2m_4m_3} - M^{I}_{m_1m_2m_3m_4}\big)\Big]. \tag{A7}$$

A major obstacle in the LSDA + U method is that the electronic interactions are already partially included in the LSDA energy thus a simple addition of the term E^{HF} to the LSDA energy would lead to DC. An ideal DC term should subtract the mean-field part from the HF term, leaving only an orbital-dependent correction to the orbital-independent LSDA potential.[64]

Two main approximations for the DC term exist in the literature: the first one is realistic for weakly correlated systems and would become exact in the case of uniform occupation numbers (around mean field).[66] The second one is the fully localized limit (FLL) DC term proposed by Lichtenstein *et al.*[13] This term describes very localized systems with integer occupation numbers. The FLL DC term is constructed from Eq. (A7) by the two simplifications: (1) one assumes fully occupied orbitals,

$$n^{I\sigma}_{mm'} = \delta_{mm'}.$$

(2) The matrix elements are approximated by averaged matrix elements:

$$M^{I}_{mm'mm'} = \underbrace{\frac{1}{(2l+1)^2}\sum_{mm'} M^{I}_{mm'mm'}}_{:=U^I}, \tag{A8}$$

$$M^{I}_{mm'm'm} = \underbrace{\frac{1}{2l\,(2l+1)}\sum_{m\neq m'} M^{I}_{mm'm'm}}_{:=J^I}. \tag{A9}$$

The DC term in the FLL is

$$E^{\mathrm{DC}} = \sum_{I}\left[\frac{U^I}{2}N^I(N^I-1) - \frac{J^I}{2}\sum_{\sigma}N^{I\sigma}(N^{I\sigma}-1)\right], \tag{A10}$$

where $N^{I\sigma} = \sum_m n^{I\sigma}_{mm}$ and $N^I = \sum_\sigma N^{I\sigma}$. Instead of E^{LSDA}, also other local/semilocal exchange-correlation functionals can be used in Eq. (A1). A frequent choice is the generalized gradient approximation, in this case, the method is called GGA + U.

2. Screening effects

In the previous section, the total energy of the LSDA + U method was derived. One could use atomic basis functions to evaluate the matrix elements in Eq. (A7) and for the determination of U^I and J^I in Eqs. (A8) and (A9). But this would totally neglect the screening of the bare Coulomb interaction. Hence, the matrix elements are replaced by parameters. These parameters are chosen in such a way that they allow for many-body (screening) effects. For the Coulomb interaction, the matrix elements can be written as[67]

$$M^{I}_{m_1m_2m_3m_4} = \sum_{k=0}^{2l} a_k\,(m_1m_3m_2m_4)\,F^I_k, \tag{A11}$$

where the $a_k(m_1m_3m_2m_4)$ are real numbers given by

$$a_k = \sum_{L=0}^{2l}\sum_{M_L=-L}^{L}(-1)^L(2l+1)^2(2L+1)\begin{pmatrix} l & k & l\\ 0 & 0 & 0\end{pmatrix}^2 \times \begin{pmatrix} l & l & L\\ m_1 & m_2 & -M_L\end{pmatrix}\begin{pmatrix} l & l & L\\ m_3 & m_4 & -M_L\end{pmatrix}^* \times \begin{Bmatrix} l & l & k\\ l & l & L\end{Bmatrix}. \tag{A12}$$

Here, $\begin{pmatrix}\cdots\\ \cdots\end{pmatrix}$ denotes a Wigner $3-j$ symbols and $\begin{Bmatrix}\cdots\\ \cdots\end{Bmatrix}$ is the Wigner $6-j$ symbols. It is worth analyzing the squared $3-j$ symbol[68]

$$\begin{pmatrix} l & k & l\\ 0 & 0 & 0\end{pmatrix}^2 = \frac{1}{2}\int_{-1}^{1} d\zeta\, P_l(\zeta)\,P_k(\zeta)\,P_l(\zeta)\,d\zeta. \tag{A13}$$

The integral of the three Legendre polynomials vanishes if $l+k+l$ is odd and hence

$$a_k\,(m_1m_3m_2m_4) = \begin{cases} 0 & \text{if } k \text{ is odd,}\\ \text{given by Eq. (12).}\end{cases}$$

This means that only the Slater integrals F^I_k with even k are needed in Eq. (A11). The Slater integrals represent the radial part of the Coulomb interaction, which is mostly affected by screening effects. Hence they are replaced by "screened Slater integrals" $\{S^I_0, S^I_2, \ldots, S^I_{2l}\}$. These are the parameters of the LSDA + U scheme. In practice, these screened Slater integrals are usually reexpressed in terms of only two parameters:[13] (1) U^I the screened averaged Coulomb on-site repulsion and (2) J^I the screened exchange interaction.

Note that the DC term in Eq. (A10) is already expressed in terms of U^I and J^I. If the orbital quantum number l is two or greater, additional conditions are needed to ensure a unique map between $\{S^I_0, S^I_2, \ldots, S^I_{2l}\}$ and $\{U^I, J^I\}$.

For all transition metals ($l=2$), the ratio of the atomic Slater integral F^I_4/F^I_2 is constant with good accuracy (for all TMOs, the ratio is between 0.62 and 0.63).[69] Screening should affect F^I_4 and F^I_2 in equal measure, hence the ratio $S^I_4/S^I_2 = 0.625 = 5/8$ is used as the condition. The relations between $\{S^I_0, S^I_2, S^I_4\}$ and $\{U^I, J^I\}$ are

$$S^I_0 = U^I, \tag{A14}$$

$$S^I_2 = \frac{112}{13}J^I, \tag{A15}$$

$$S^I_4 = \frac{70}{13}J^I. \tag{A16}$$

3. The choice of the parameters (U^I, J^I)

At this point, it is worth discussing how the values for the two parameters, U^I and J^I, are actually obtained. As was

discussed in Sec. V B, a direct calculation of the parameters with the Eqs. (A8) and (A9) and the unscreened Slater integrals $\{F_k^I\}$ would lead to an overestimation of the Coulomb repulsion ($U^I = 15$–20 eV) and the exchange interaction, due to the lack of screening. Hence a different approach must be used to obtain these parameters. In practice, two main approaches exist. (1) The first method is to chose the parameter in such a way to reproduce as many experimental observables as possible. This approach is frequently applied to large systems, where calculation of U^I and J^I is difficult. (2) The second way is to calculate the parameters U^I and J^I *ab initio*. This brings the "first-principles" character back to the LSDA + U method.

For such a calculation two schemes are used: (1) originally the value of U^I was chosen based on a constrained LSDA calculation,[9] and (2) a newer method is the linear response approach, which leads to smaller values of U^I compared the constrained LSDA.[16]

4. Analysis of the LSDA + U method

To get a more transparent physical interpretation of the LSDA + U method, it is worth trying to reduce the complexity of the current formalism. We consider a system with strongly correlated d electrons. The simplification consists of neglecting the higher screened Slater integrals S_2^I and S_4^I, which is equivalent to setting J^I to zero. Note that S_2^I and S_4^I are not necessarily smaller than S_0^I. For instance, in the case of TMOs, they are all of the same order. (See Eqs. (A14), (A15), and (A16) with the value $U/J \approx 9$ obtained by constraint LSDA.[9])

However, to get an insight into the LSDA + U method, such a simplified analysis is instructive. In this approximation, the energy functional of Eq. (A1) simplifies to[16]

$$E^{\mathrm{U}} = \sum_I \sum_\sigma \sum_{mm'} \frac{U^I}{2}\left[\delta_{mm'} n^{I\sigma}_{mm'} - n^{I\sigma}_{mm'} n^{I\sigma}_{m'm}\right].$$

The potential acting on Kohn-Sham orbital φ_i reduces in this simple approach to

$$\sum_I \sum_{mm'} \left[\frac{U^I}{2}\left(1 - 2n^{I\alpha}_{mm'}\right)\right] \langle I,m'\alpha|\varphi_i\rangle \langle \mathbf{r}\alpha|I,m\alpha\rangle. \quad \text{(A17)}$$

The most important properties of the potential are as follows: (1) because of the projector $\langle I,m'\alpha|\varphi_i\rangle$ in Eq. (A17), Kohn-Sham orbitals with mainly s or p character are unaffected. To treat only d electrons with the E^{U} term was one of the main ideas behind the LSDA + U method. (2) Since there is no Fermi function in the potential, unoccupied Kohn-Sham orbitals are also affected. (3) Kohn-Sham orbitals with d character are shifted away from the Fermi energy. Depending on the occupation number, the orbitals are shifted either up ($n^{I\alpha}_{mm} < 1/2$) or down ($n^{I\alpha}_{mm} > 1/2$) in energy with the size of the shift proportional to U^I. This leads to a gap opening. (4) The potential is nonlocal like the HF potentials and diagonal in spin space. (5) Besides the two parameters U^I and J^I, the whole method depends also on the choice of an atomic basis set (because the occupation numbers $\{n^{I\sigma}_{mm'}\}$ refer to these basis functions).

[1] N. F. Mott, Proc. Phys. Soc. London, Sect. A **62**, 416 (1949).
[2] P. Mori-Sanchez, A. J. Cohen, and W. Yang, Phys. Rev. Lett. **100**, 146401 (2008).
[3] K. Terakura, T. Oguchi, A. R. Williams, and J. Kübler, Phys. Rev. B **30**, 4734 (1984).
[4] Z. Szotek, W. M. Temmerman, and H. Winter, Phys. Rev. B **47**, 4029 (1993).
[5] G. Fischer, M. Däne, A. Ernst, P. Bruno, M. Lüders, Z. Szotek, W. Temmerman, and W. Hergert, Phys. Rev. B **80**, 014408 (2009).
[6] C. Rödl, F. Fuchs, J. Furthmüller, and F. Bechstedt, Phys. Rev. B **79**, 235114 (2009).
[7] C. Franchini, V. Bayer, R. Podloucky, J. Paier, and G. Kresse, Phys. Rev. B **72**, 045132 (2005).
[8] X. B. Feng, Phys. Rev. B **69**, 155107 (2004).
[9] V. I. Anisimov, J. Zaanen, and O. K. Andersen, Phys. Rev. B **44**, 943 (1991).
[10] V. I. Anisimov, M. A. Korotin, A. S. Mylnikova, A. V. Kozhevnikov, D. M. Korotin, and J. Lorenzana, Phys. Rev. B **70**, 172501 (2004).
[11] A. N. Yaresko, V. N. Antonov, and B. N. Harmon, Phys. Rev. B **68**, 214426 (2003).
[12] T. Cai *et al.*, Physica B **404**, 89 (2008).
[13] A. I. Liechtenstein, V. I. Anisimov, and J. Zaanen, Phys. Rev. B **52**, R5467 (1995).
[14] A. G. Petukhov, I. I. Mazin, L. Chioncel, and A. I. Lichtenstein, Phys. Rev. B **67**, 153106 (2003).
[15] S. L. Dudarev, G. A. Botton, S. Y. Savrasov, C. J. Humphreys, and A. P. Sutton, Phys. Rev. B **57**, 1505 (1998).
[16] M. Cococcioni and S. de Gironcoli, Phys. Rev. B **71**, 035105 (2005).
[17] E. Bousquet and N. Spaldin, Phys. Rev. B **82**, 220402 (2010).
[18] J. B. Bennemann and K. H. Ketterson, *The Physics of Superconductors Vol I: Conventional and High-Tc Superconductors* (Springer, Berlin, Heidelberg, 2002).
[19] D. Manske, *Theory of Unconventional Superconductors* (Springer-Verlag, Berlin, Heidelberg, 2004).
[20] D. Muñoz, F. Illas, and I. de P. R. Moreira, Phys. Rev. Lett. **84**, 1579 (2000).
[21] R. Ofer, G. Bazalitsky, A. Kanigel, A. Keren, A. Auerbach, J. S. Lord, and A. Amato, Phys. Rev. B **74**, 220508 (2006).
[22] E. Dagotto, Rev. Mod. Phys. **66**, 763 (1994).
[23] N. Lee, P. A. Nagaosa, and W. X. G., Rev. Mod. Phys. **78**, 17 (2006).
[24] O. Bengone, M. Alouani, P. Blöchl, and J. Hugel, Phys. Rev. B **62**, 16392 (2000).
[25] M. J. Han, T. Ozaki, and J. Yu, Phys. Rev. B **73**, 045110 (2006).
[26] S. L. Dudarev, L.-M. Peng, S. Y. Savrasov, and J.-M. Zuo, Phys. Rev. B **61**, 2506 (2000).
[27] I. I. Mazin and V. I. Anisimov, Phys. Rev. B **55**, 12822 (1997).
[28] I. V. Solovyev and K. Terakura, Phys. Rev. B **58**, 15496 (1998).
[29] X. Wan, Q. Yin, and S. Y. Savrasov, Phys. Rev. Lett. **97**, 266403 (2006).
[30] O. Grotheer, C. Ederer, and M. Fähnle, Phys. Rev. B **63**, 100401 (2001).

[31]P. Buczek, A. Ernst, P. Bruno, and L. M. Sandratskii, Phys. Rev. Lett. **102**, 247206 (2009).
[32]E. K. U. Gross and W. Kohn, Phys. Rev. Lett. **55**, 2850 (1985).
[33]S. V. Halilov, H. Eschrig, A. Y. Perlov, and P. M. Oppeneer, Phys. Rev. B **58**, 293 (1998).
[34]P. W. Anderson, *Theory of Magnetic Exchange Interactions: Exchange in Insulators and Semiconductors*, Solid State Physics Vol. 14, 1st ed. (Academic Press, New York, 1963).
[35]M. Pajda, J. Kudrnovský, I. Turek, V. Drchal, and P. Bruno, Phys. Rev. B **64**, 174402 (2001).
[36]J. Rusz, I. Turek, and M. Divis, Phys. Rev. B **71**, 174408 (2005).
[37]D. J. Singh and L. Nordström, *Planewaves, Pseudopotentails and the LAPW method*, 2nd ed. (Kluwer Academic, Boston, Dordrecht, London, 2005).
[38]ELK code (2004) [http://elk.sourceforge.net].
[39]R. W. G. Wyckoff, *Crystal structures*, 2nd ed. (Interscience, New York, 1965), Vol 1.
[40]A. K. Cheetham and D. A. O. Hope, Phys. Rev. B **27**, 6964 (1983).
[41]W. Jauch, M. Reehuis, H. J. Bleif, F. Kubanek, and P. Pattison, Phys. Rev. B **64**, 052102 (2001).
[42]J. P. Perdew and Y. Wang, Phys. Rev. B **45**, 13244 (1992).
[43]J. P. Perdew, K. Burke, and M. Ernzerhof, Phys. Rev. Lett. **77**, 3865 (1996).
[44]Z. V. Popović *et al*., Phys. Rev. B **63**, 165105 (2001).
[45]H. Nakamuraa, N. Hayashia, N. Nakaia, M. Okumura, and M. Machida, Physica C **496**, 908 (2009).
[46]R. J. Powell and W. E. Spicer, Phys. Rev. B **2**, 2182 (1970).
[47]G. A. Sawatzky and J. W. Allen, Phys. Rev. Lett. **53**, 2339 (1984).
[48]J. van Elp, J. L. Wieland, H. Eskes, P. Kuiper, G. A. Sawatzky, F. M. F. de Groot, and T. S. Turner, Phys. Rev. B **44**, 6090 (1991).
[49]M. Gvishi and D. Tannhausera, J. Phys. Chem. Solids **33**, 893 (1972).
[50]H. K. Bowen, D. Adler, and B. H. Auker, J. Solid State Chem. **12**, 355 (1975).
[51]R. N. Iskenderov, I. A. Drabkin, L. T. Emel'yanova, and Y. M. Ksendzov, Fiz. Tverd. Tela (Leningrad) **10**, 2573 (1968).
[52]J. van Elp, R. H. Potze, H. Eskes, R. Berger, and G. A. Sawatzky, Phys. Rev. B **44**, 1530 (1991).
[53]I. A. Drabkin, L. T. Emel'yanova, R. N. Iskenderov, and Y. M. Ksendzov, Fiz. Tverd. Tela (Leningrad) **10**, 3082 (1968).
[54]S. Massidda, A. Continenza, M. Posternak, and A. Baldereschi, Phys. Rev. Lett. **74**, 2323 (1995).
[55]S. Kobayashi, Y. Nohara, S. Yamamoto, and T. Fujiwara, Phys. Rev. B **78**, 155112 (2008).
[56]W. L. Roth, Phys. Rev. **110**, 1333 (1958).
[57]D. C. Khan and R. A. Erickson, Phys. Rev. B **1**, 2243 (1970).
[58]D. Herrmann-Ronzaud, P. Burlet, and J. Rossat-Mignod, J. Phys. C **11**, 2123 (1978).
[59]E. Sjöstedt, *Aufmented Planewaves, Developments and Applications to Magnetism*, 2nd ed. (Eklundshofs Grafiska AB, Uppsala, 2002).
[60]P. Rivero, I. P. R. Moreira, G. E. Scuseria, and F. Illas, Phys. Rev. B **79**, 245129 (2009).
[61]S. Tomizasu, K. Itoh, JPSJ **75**, 084708 (2006).
[62]M. T. Hutchings and E. J. Samuelsen, Phys. Rev. B **6**, 3447 (1972).
[63]G. Pepy, J. Phys. Chem. Solids **35**, 433 (1973).
[64]F. Bultmark, F. Cricchio, O. Grånäs, and L. Nordström, Phys. Rev. B **80**, 035121 (2009).
[65]I. V. Solovyev, A. I. Liechtenstein, and K. Terakura, Phys. Rev. Lett. **80**, 5758 (1998).
[66]M. T. Czyzyk and G. A. Sawatzky, Phys. Rev. B **49**, 14211 (1994).
[67]B. R. Judd, *Operator Techniques in Atomic Spectroscopy*, 1st ed. (McGraw-Hill, New York, 1963).
[68]G. Racah, Phys. Rev. **62**, 438 (1942).
[69]F. M. F. de Groot, J. C. Fuggle, B. T. Thole, and G. A. Sawatzky, Phys. Rev. B **42**, 5459 (1990).